The Impact of Divergence Tilt and Meridional Flow for Cross-Equatorial Eddy Momentum Transport in Gill-Like Settings

PABLO ZURITA-GOTOR

Universidad Complutense and Instituto de Geociencia UCM-CSIC, Madrid, Spain

(Manuscript received 7 June 2019, in final form 20 December 2019)

ABSTRACT

This work investigates the sensitivity of the cross-equatorial eddy momentum flux and its rotational and divergent components to Hadley cell strength in simple variants of the Gill problem. An expression is derived linking the divergent momentum flux to the mean meridional wavenumber weighted by the spectrum of divergent eddy kinetic energy, supporting the relation between divergence phase tilt and momentum flux suggested by a previous study. Newtonian cooling makes the divergence tilt eastward moving away from the equator as observed, but this tilt is also sensitive to the Hadley cell. As the divergence tilt is enhanced in the downstream direction of the flow, wave propagation increases along that direction when the Hadley cell strengthens. The meridional flow also plays a second, important role for cross-equatorial propagation. With no Hadley cell, inviscid Sverdrup balance requires perfect compensation between the divergent and rotational momentum fluxes at the equator. The model can only produce cross-equatorial propagation when Sverdrup balance is violated, which in the linear, nearly inviscid limit requires vorticity advection by the mean flow. As the Hadley cell attenuates the geopotential tilt imparted by the divergent forcing, the compensation by the rotational momentum flux is reduced. The linear model can reproduce reasonably well previous nonlinear results by Kraucunas and Hartmann when linearized about their zonal-mean climatologies. The sensitivity of the cross-equatorial momentum fluxes to Hadley cell strength in these solutions is dominated by changes in the divergent flux and consistent with diagnosed changes in the divergence tilt.

1. Introduction

It has been known for some time that the momentum transport by tropical eddies plays a first-order role for the determination of the mean tropical winds in the terrestrial atmosphere (Lee 1999). Dima et al. (2005) performed a comprehensive analysis of the tropical momentum budget in NCEP reanalysis and showed that the stationary (climatological seasonal-mean) tropical eddies transport westerly momentum into the equator in the annual mean and from the winter to the summer hemisphere during the solstices. They proposed that the momentum transport could be associated with the atmospheric response to asymmetric tropical heating. This is supported by findings from aquaplanet simulations with zonally varying SST in the Northern Hemisphere subtropics, which also produce cross-equatorial eddy momentum transport in a solstitial setting (Shaw 2014).

The fact that zonally localized tropical heating may give rise to equatorward momentum transport is also well known from idealized studies (Suarez and Duffy 1992; Kraucunas and Hartmann 2005). Beyond the terrestrial atmosphere, this forcing is thought to be responsible for the superrotation of tidally locked planets due to their strong day–night heating contrast (Merlis and Schneider 2010; Showman and Polvani 2011). Although the eddy acceleration has been traditionally attributed to the meridional propagation of Rossby waves forced by the heating (Held 1999; Laraia and Schneider 2015), Showman and Polvani (2011, hereafter SP11) proposed an alternative mechanism involving the interaction between the Rossby and Kelvin components of the Matsuno–Gill response. This interaction has also been found to induce equatorward momentum transport and superrotation in the absence of external forcing (Zurita-Gotor and Held 2018).

A key difference between tropical and extratropical eddy-driven jets is the role played by the divergent flow.

Denotes content that is immediately available upon publication as open access.

Corresponding author: Pablo Zurita-Gotor, pzurita@alum.mit.edu

DOI: 10.1175/JAS-D-19-0158.1

Extratropical eddy-driven jets are driven by vorticity mixing and vorticity fluxes and can be understood in terms of purely rotational dynamics (Vallis 2017). In contrast, in both SP11 and Zurita-Gotor and Held (2018) the zonal acceleration is due to vertical rather than meridional momentum advection (see also Showman and Polvani 2010). Zurita-Gotor (2019a) showed that the same is true in the deep Earth tropics, in which the eddy acceleration is dominated by the convergence of the *divergent* momentum flux $\overline{u_r'v_d'}$ (we use overbars and primes to denote the zonal mean and eddy deviations, while the r and d subscripts indicate rotational and divergent components).

Motivated by these observations, Zurita-Gotor (2019b, hereafter Z19b) studied the determination of the divergent momentum flux. The direction of this flux depends on the phase relation between the rotational and divergent anomalies rather than on the meridional tilt of the streamlines as is the case for the traditional rotational momentum flux $\overline{u_r'v_r'}$. Z19b found that the observed seasonal cycle of $\overline{u_r'v_d'}$ was well reproduced when the observed divergent flow was used to force the vorticity equation, suggesting that this momentum flux could be regarded as a forced response. He also noted that the direction of $\overline{u_r'v_d'}$ was primarily controlled by the meridional tilt of the large-scale divergence field in his model and interpreted this result using the vorticity balance.

Figure 1 shows the observed structure of the $k = 1$ stationary wave using ERA-Interim data (Dee et al. 2011) during the years 1979–2016, integrated between 150 and 300 hPa. The left panels show with contours the seasonal-mean geopotential height and with shading the large-scale divergence, coarse grained to eliminate the fine ITCZ structure (meridional wavenumbers $|l| > 3$ have been filtered out). We can see that the divergence field tilts eastward with latitude moving away from its maximum near the equator in the summer hemisphere during all seasons. To our knowledge, this robust divergence pattern is not broadly recognized in the literature, except for its regional manifestations during austral summer: the South Pacific and South Atlantic convergence zones (e.g., Van Der Wiel et al. 2015). However, as Fig. 1 shows, a similar tilt is detectable in the Northern Hemisphere and/or during other seasons when the fine ITCZ structure is filtered out. The robustness of the divergence tilt suggests that it has a dynamical rather than geographical origin, which is consistent with idealized studies of the South Pacific convergence zone (Van Der Wiel et al. 2016).

The observed seasonal cycle of the eddy momentum flux is consistent with this structure. During DJF, when the wave source shifts into the Southern Hemisphere, the southward cross-equatorial momentum flux into that latitude (Fig. 1c) is consistent with the southwest-to-northeast divergence tilt found over the propagation region. Reversibly, when the wave source moves to the Northern Hemisphere during JJA, the northward cross-equatorial momentum flux (Fig. 1f) is consistent with the northwest-to-southeast tilt to its south. During both seasons, the momentum flux is dominated by its divergent component (red lines) as noted above.

The weak eddy momentum flux sensitivity on the mean flow found by Z19b is at odds with previous nonlinear shallow-water results by Kraucunas and Hartmann (2007, hereafter KH07), who found that the interhemispheric eddy momentum flux in their model was enhanced by the cross-equatorial Hadley cell. Z19b speculated that his different results might be due to the use of a weak temperature gradient approximation (WTG; Sobel et al. 2001), in which the eddy divergence is kept fixed as the meridional flow is changed. The impact of the Hadley cell on the eddy momentum flux might be larger if the meridional flow also affected the divergence, for instance modulating its tilt. A cursory inspection of the KH07 results lends some credence to this idea, as their simulations with large cross-equatorial momentum transport have a more pronounced divergence tilt (cf. their Figs. 2f and 5f to their Figs. 2c and 5c). The eddy momentum flux and the divergence tilt are both enhanced with a Hadley cell (their Fig. 5f).

The goal of this study is to investigate the sensitivity of the eddy momentum flux in simple variants of the classical Gill (1980) model, in an attempt to reconcile the conflicting results of Z19b and KH07. The model is described in section 2, and sections 3–5 present the main results. Section 3 addresses the WTG limit, in which the divergence field is constrained by the prescribed heating. Section 4 investigates the impact of thermal damping on the solutions–a key difference is that the divergence field is now internally determined. Section 5 moves away from the homogeneous framework to replicate and analyze the results of KH07. Section 6 concludes with a summary.

2. Model formulation

The Gill (1980) model consists of the shallow-water momentum and continuity equations on an equatorial beta plane, linearized about a resting basic state and forced by prescribed heating. In its original formulation, Gill's equations were derived for the first baroclinic mode using a vertical modal decomposition. However, equivalent equations can be derived under alternative

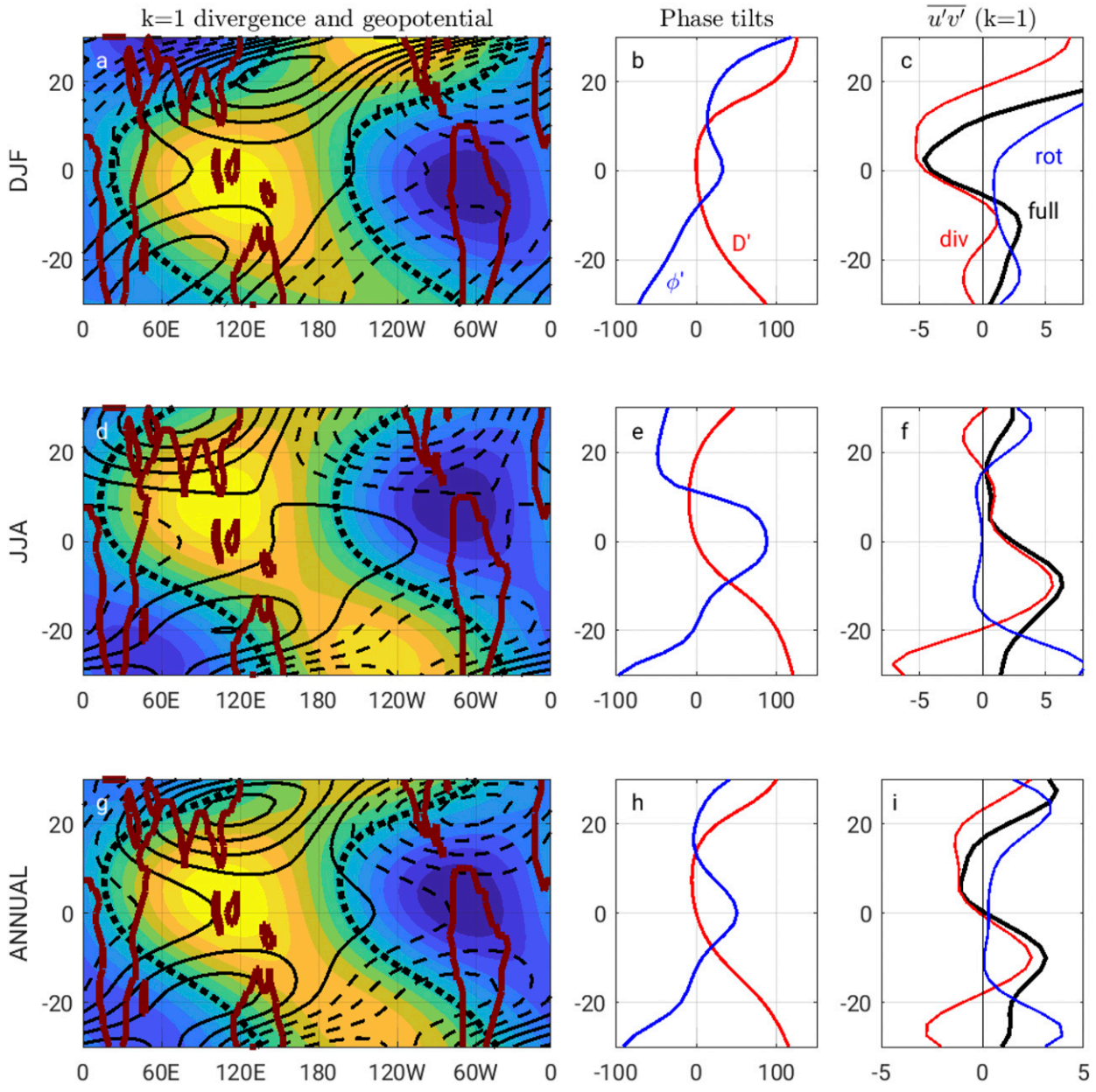

FIG. 1. (a) Coarse-grained ($|l| \leq 3$) upper-level (150–300 hPa) divergence (shading; zero contour shown with thick dotted line) and geopotential (contours; negative dashed) for the gravest zonal harmonic ($k = 1$) during DJF. (b) Phase shifts of divergence D' (red) and geopotential ϕ' (blue) as a function of latitude for the same data in (a). Positive (negative) values indicate phase leads (lags) relative to the phase of D' at the equator. (c) Total eddy momentum flux (black) and rotational (blue) and divergent (red) contributions. (d)–(f) As in (a)–(c), but during JJA. (g)–(i) As in (a)–(c), but for the annual mean.

frameworks. For instance, Neelin (1988) applied these equations to model the boundary layer flow, in which context the use of strong friction (required for realistic solutions) is more palatable.

Because this study focusses on the determination of the upper-troposphere eddy momentum fluxes, our equations are meant to model an upper-troposphere isentropic layer instead. Additionally, we linearize the equations about a background meridional flow V motivated by the presumed impact of the Hadley cell on meridional propagation and eddy momentum fluxes (Kraucunas and Hartmann 2007). The governing forced, steady equations are

$$-\beta y v' + V\frac{\partial u'}{\partial y} = -\frac{\partial \phi'}{\partial x} - a u', \tag{1a}$$

$$\beta y u' + V\frac{\partial v'}{\partial y} = -\frac{\partial \phi'}{\partial y} - a v', \tag{1b}$$

$$D' = Q' - \frac{b}{c^2}\phi'. \tag{1c}$$

Here u' and v' are the horizontal eddy velocities and $D' = \partial_x u' + \partial_y v'$ is the horizontal eddy divergence, $\phi' = gh'$ is geopotential (h' is the shallow-water depth), and $Q' = \tilde{Q}'/H$ represents the prescribed mass source forcing the model, where $\tilde{Q}'$ is the heating and H is the mean layer depth, which we may regard as a measure of the stratification. This parameter is expressed in terms of the gravity wave speed $c = \sqrt{gH}$ above, while a and b are the mechanical and thermal damping rates, respectively. For simplicity, we only include the meridional advection by the Hadley cell in the momentum equations (sensitivity experiments suggest a weak impact on the continuity equation).

The momentum equations are easily combined to produce the vorticity equation:

$$\beta y D' + \beta v' + V\frac{\partial \xi'}{\partial y} + a\xi' = 0, \tag{2}$$

where $\xi' = \partial_x v' - \partial_y u'$ is relative vorticity. In the inviscid limit $a = 0$ and with no meridional flow, this equation reduces to simple Sverdrup balance: $v' = -yD'$. In this limit, the solution can be calculated analytically as shown by SP11 (their appendix C).

In other cases, the solutions must be found numerically. Our solution method follows Bretherton and Sobel (2003). We first eliminate the vorticity in Eq. (2) using the definition of divergence to find the following expression relating v' and D':

$$[\beta\partial_x + (V\partial_y + a)\nabla^2]v' = (V\partial_{yy} + a\partial_y - \beta y\partial_x)D'. \tag{3}$$

Here, we consider two cases. With no Newtonian cooling ($b = 0$), Eq. (1c) reduces to $D' = Q'$, which we can substitute above to solve for v' given Q'. Bretherton and Sobel (2003) refer to this as the WTG limit. Because the divergence field is directly prescribed, this limit provides a useful device for testing the sensitivity of the eddy momentum fluxes on the divergence tilt suggested by our previous work. This is done in section 3.

With nonzero b, we combine the momentum equations to find a relation between ϕ' and v', which we can use to eliminate ϕ' in Eq. (1c) following Bretherton and Sobel (2003). Substituting in Eq. (3), we then get a closed expression for v'. In this general case, the divergence is internally determined and may develop meridional tilts even when the heating does not tilt. Section 4 studies this limit aiming to understand the determination of the divergence tilt in our model.

To replicate the results of KH07, we also consider in section 5 an inhomogeneous formulation with nonzero zonal wind and latitude-dependent $U(y)$, $V(y)$, and $H(y)$ diagnosed from their climatologies. The resulting system of linearized equations must be solved numerically.

In all these cases, it is trivial after solving for v' to calculate all other variables and the eddy momentum flux $\overline{u'v'}$. We can also decompose this momentum flux as

$$\overline{u'v'} = \overline{u'_r v'_r} + \overline{u'_r v'_d} + \overline{u'_d v'_r} + \overline{u'_d v'_d}, \tag{4}$$

following Zurita-Gotor (2019a). As discussed in that work, the first two components on the right-hand side dominate. We will refer to them as the rotational and divergent eddy momentum fluxes.

Motivated by the observations showing that the eddy momentum flux is dominated by the gravest ($k = 1$) zonal harmonic (Zurita-Gotor 2019a), we force this single wavenumber instead of using localized heating as most previous studies. The forcing is defined by the following expression:

$$Q' = Q_0 \cos(kx + \ell y)e^{-(y-y_0)^2/(2\lambda^2)}, \tag{5}$$

where $\lambda = (c/\beta)^{1/2}$ is the equatorial deformation radius. We use a forcing amplitude $Q_0 = 1.5 \times 10^{-6}\,\mathrm{s}^{-1}$, which is on the order of the observed $k = 1$ eddy divergence in the upper troposphere.

To produce cross-equatorial eddy momentum fluxes Q' needs to be asymmetric about the equator. Traditionally, this has been achieved by shifting the heating off the equator or adding an antisymmetric component to Q'. An alternative way to break the symmetry is by tilting the heating meridionally using a nonzero ℓ. Motivated by the results of Z19b and the structure of the observed divergence field in Fig. 1, this will be our preferred method to introduce asymmetry in the WTG limit. With $\ell < 0$ ($\ell > 0$), the heating exhibits a southwest-to-northeast (northwest-to-southeast) tilt as observed during DJF (JJA) over the propagation region. Focusing on JJA, we take as a typical value for the tilt $\ell = \pi/(5\lambda)$, which produces the heating pattern shown with shading in Fig. 2a. We will refer to this value of ℓ as the "control westward tilt."

We solve the above equations numerically, using a spectral decomposition in x and finite differences in y in a rectangular domain with size $L_x \times L_y$, where $L_x = 2\pi a$ and $L_y = 60\lambda$. Using $\beta = 2\Omega/a$ (Ω and a are the terrestrial rotation rate and radius) and a typical

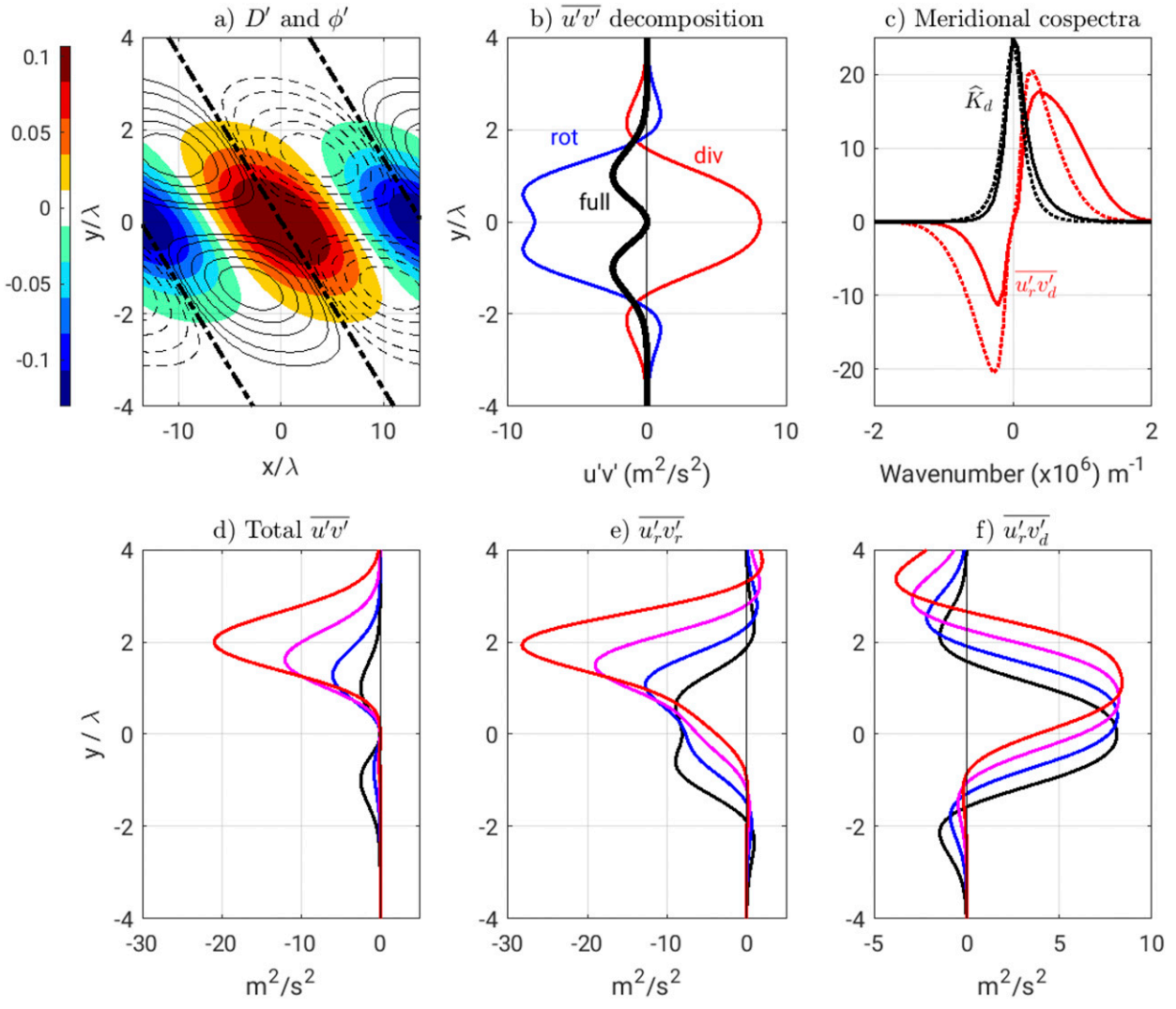

FIG. 2. (a) Divergence (shading; day^{-1}) and geopotential (contours) for the adiabatic, inviscid problem with a resting basic state and the control westward tilt. (b) Net eddy momentum flux $\overline{u'v'}$ (thick black) and rotational ($\overline{u'_r v'_r}$; blue) and divergent ($\overline{u'_r v'_d}$; red) contributions. (c) Divergent eddy kinetic energy spectra (black lines) and meridional cospectra of $u'_r v'_d$ (red lines; scale is arbitrary) for the untilted problem (dotted) and with the control westward tilt (solid). (d) Total eddy momentum fluxes and (e) rotational and (f) divergent contributions in adiabatic, inviscid solutions with the control westward tilt and $y_0/\lambda = 0$ (black), 0.5 (blue), 1 (magenta), and 1.5 (red).

gravity wave speed $c = 50\,\mathrm{m\,s^{-1}}$, the deformation radius is $\lambda \approx 1500\,\mathrm{km}$. These are the same parameters used by Bretherton and Sobel (2003). With $V = 0$ the solutions of these equations are known to be meridionally trapped (Matsuno 1966) but with nonzero V meridional propagation is allowed (Schneider and Watterson 1984), which may give rise to resonance with rigid walls. A sponge damps the eddies near the walls to prevent backward reflection and resonance. Sensitivity experiments changing the meridional domain size and resolution (NY = 760) and the sponge damping rate have shown our results to be robust. When thermal or frictional damping are included, we take as reference, control values the same damping rates as Bretherton and Sobel (2003): $a = b = 0.15c/\lambda$.

3. The WTG limit

In the WTG limit the divergence field is directly determined by the heating. Consider first the inviscid case $a = 0$ in a resting basic state ($V = 0$). With untilted heating, both the rotational and divergent components of $\overline{u'v'}$ vanish (not shown). The vanishing of the divergent momentum flux is consistent with the arguments of Z19b, who note that for a single wave with meridional wavenumber l the direction of $\overline{u'_r v'_d}$ depends on the sign

of $\omega_0 l$, where $\omega_0(k, l)$ is the free mode frequency, westward for the dominant grave modes. Appendix A generalizes this result with a full meridional wave spectrum and shows that in a resting basic state the domain-integrated eddy momentum flux by zonal wavenumber k is given by

$$\langle \overline{u_r' v_d'}(k) \rangle = \frac{2}{k} \int_{-\infty}^{\infty} l \hat{K}_d(k, l)\, dl, \tag{6}$$

where $\hat{K}_d(k, l)$ is the spectrum of the divergent eddy kinetic energy $K_d = (1/2)(\mathbf{u}_d' \cdot \mathbf{u}_d')$.

Consistent with this result, with the control westward-tilted heating (shading in Fig. 2a) the divergent momentum flux is northward (Fig. 2b, red line), as the forcing biases the $\hat{K}_d$ spectrum toward positive l (cf. the solid and dotted black lines in Fig. 2c). The meridional $\overline{u_r' v_r'}$ cospectrum (red lines in Fig. 2c) shows that while the positive and negative momentum fluxes cancel out with untilted heating, the positive fluxes dominate with the westward $\hat{K}_d$ bias.

However, the *full* eddy momentum flux has a very different structure due to the impact of the rotational component $\overline{u_r' v_r'}$ (Fig. 2b). At the equator, both $\overline{u'v'}$ and its convergence vanish, with the momentum flux becoming negative at some distance. Z19b focused on the determination of $\overline{u_r' v_d'}$ because this component strongly dominates in the deep tropics in observations. In contrast, strong compensation between the rotational and divergent components is produced by our model. Perfect compensation is found at the equator, where Sverdrup balance $v' = -yD'$ implies $v' = 0$. Cross-equatorial propagation requires violation of Sverdrup balance, or an equatorial vorticity source.

Kinematically, we can understand the sign of $\overline{u_r' v_r'}$ by noting that the structure of the rotational response is constrained by the heating tilt. It is easy to show that in the absence of friction and meridional flow, the tilt of the streamfunction response agrees with that of the Rossby wave source, so we expect $\overline{u_r' v_d'}$ and $\overline{u_r' v_r'}$ to point in opposite directions due to their opposite sensitivity on meridional wavenumber. As $\overline{u_r' v_d'}$ and $\overline{u_r' v_r'}$ compensate at the equator, the rotational momentum flux dominates at higher latitudes due to the enhanced Rossby wave source. Figures 2d–f describe the sensitivity of the eddy momentum fluxes to the heating latitude. With increasing latitude, the rotational momentum flux increases significantly in the forced hemisphere, while the divergent momentum flux only shifts. The net momentum flux is dominated by the rotational component in the forced hemisphere, with perfect compensation between $\overline{u_r' v_d'}$ and $\overline{u_r' v_r'}$ at the equator as before.

In the next subsections, we discuss two processes that may be important for violating Sverdrup balance and weakening the rotational momentum flux in observations.

a. *Violation of Sverdrup balance: The impact of friction*

It is well recognized that linear tropical models need strong friction to produce a realistic circulation, which has been traditionally attributed to the missing impact of nonlinearity (e.g., Ting and Held 1990). SP11 show that friction plays a key role for eddy momentum transport in the equatorially symmetric Gill problem. With nonzero friction, all their simulations produce eddy momentum transport into the equator due to the interaction between the Kelvin and Rossby components of the Gill response, as the differential propagation of these two waves produces an eastward tilt of the isohypses moving toward the equator (cf. Fig. 3d). Friction is essential to this mechanism because in its absence, there can be no steady Kelvin wave response[1] as the zonal momentum balance equation [Eq. (1a)] requires geopotential anomalies to vanish at the equator (Fig. 2a).

Figure 3a describes the sensitivity of the eddy momentum fluxes to friction with the control westward tilt. As friction is increased, a region of meridional eddy momentum convergence encompassing the equator appears. The eddy momentum fluxes reverse to the south of the equator and we now observe cross-equatorial propagation from the northern to the Southern Hemisphere. Looking at the partition between the rotational and divergent components, we can see that both $\overline{u_r' v_r'}$ and $\overline{u_r' v_d'}$ weaken as friction is increased (Figs. 3b,c). However, there is a clear spatial structure to the $\overline{u_r' v_r'}$ reduction that is much stronger on the south of the domain.

This spatial structure is consistent with the arguments of SP11 when applied to a tilted heating field. In particular, the differential eastward propagation by the Kelvin wave at the equator increases the northwest-to-southeast tilt imparted by the forcing to the north of the equator but opposes that tilt to the south of the equator. This is illustrated in Fig. 3 for the responses with weak (half the control value, Fig. 3d) and strong (twice the control value, Fig. 3e) heating tilts. With weak heating tilt, the geopotential tilt is dominated by the Kelvin–Rossby differential propagation and approaches the symmetric solutions of SP11. With strong heating tilt,

[1] Strictly speaking, when the response is decomposed in terms of the free modes a weak Kelvin wave component is required to balance the zonal pressure gradient by the Rossby wave at the equator. However, this response is weak and by construction cannot produce geopotential tilts.

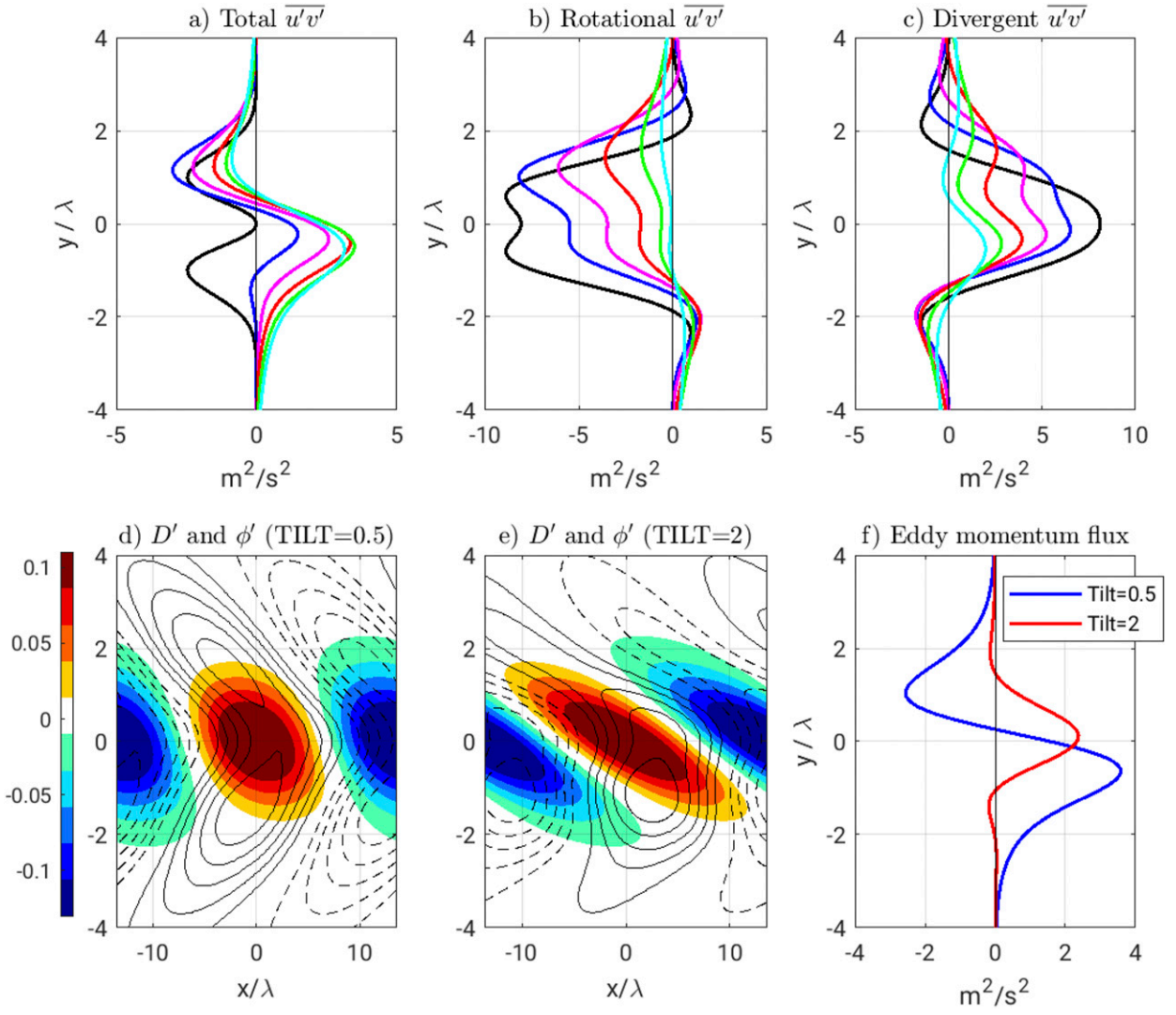

FIG. 3. (a) Total eddy momentum fluxes and (b) rotational and (c) divergent contributions in adiabatic solutions with the control westward tilt and $a/a_{\mathrm{CON}} = 0$ (black), 0.25 (blue), 0.5 (magenta), 1 (red), 2 (green), and 4 (cyan), where a_{CON} is the control friction. (d) Divergence (shading; day^{-1}) and geopotential (contours) for an adiabatic solution with the control friction and half the control tilt. (e) As in (d), but with twice the control tilt. (f) Eddy momentum flux for the responses in (d) and (e).

the geopotential tilt still reverses to the south of the equator but the tilt is much reduced due to the two competing effects. Figure 3f shows the eddy momentum flux for both cases.

To summarize, friction affects the phase tilt of the response, enhancing (reducing) the tilt imparted by the forcing on the summer (winter) side of the equator. As a result, the rotational momentum fluxes weaken on the winter side and the cross-equatorial momentum flux is dominated by the divergent component as in observations.

b. *Role of meridional flow*

It is not clear that the use of strong friction in the tropical upper troposphere is justified. Additionally, although the direction of the eddy momentum fluxes in Fig. 3 is consistent with observations, the magnitude of these fluxes is too weak. An alternative process that could violate Sverdrup balance in the inviscid limit is the meridional vorticity advection by the Hadley cell. The meridional flow breaks the symmetry of Rossby's dispersion relation and favors propagation in the direction of the flow (Schneider and Watterson 1984), which has been argued to be relevant for the cross-equatorial propagation of Rossby waves (Li et al. 2015). Z19b note that by affecting Rossby's natural frequency, the meridional flow may also shift the forced response toward meridional modes with $Vl > 0$.

The meridional Hadley flow V has a profound impact on the model's inviscid solution. Figure 4a describes the sensitivity of the momentum flux using the control westward tilt and varying southward meridional flow in the range $V = 0$–$2\,\mathrm{m\,s^{-1}}$. The negative V sustains southward propagation (positive momentum flux) that increases with V. As the solution is no longer meridionally trapped, boundary sponges are used to prevent reflection of the waves at the southern wall and ensuing resonant behavior. The sensitivity of the momentum flux is almost entirely due to the weakening of the rotational component $\overline{u_r'v_r'}$ (Fig. 4b), while the divergent momentum flux $\overline{u_r'v_d'}$ changes very little with V (Fig. 4c) consistent with Z19b. With realistic V, the rotational momentum flux becomes small and the solution is dominated by the northward divergent flux as in observations.

We can understand this sensitivity by considering how V affects Rossby's dispersion relation:

$$\omega_0(k,l;V) = Vl - \frac{\beta k}{k^2 + l^2}. \tag{7}$$

Figure 4d shows the westward Rossby frequency $-\omega_0(k = 1, l; V)$ for all values of V considered. For the longest waves ω_0 is dominated by the β term and insensitive to V, but for $|l| \gtrsim 0.5 \times 10^{-6}\,\mathrm{m^{-1}}$ modes with negative (positive) l have smaller (larger) $|\omega_0|$ and hence a stronger (weaker) response to forcing. The resonant/propagating wavenumber, defined by $\omega_0(l_0) = 0$, is negative and shifts to smaller values of $|l|$ as the southward flow strengthens.

Figure 4f shows the implications of this structure for the rotational response. The dotted black line shows the normalized divergence spectrum and the solid black line the spectrum of the Rossby wave source $F' = -\beta y D' - \beta v_d'$. Both are biased toward positive l due to the imparted southeast–northwest tilt. With a resting basic state (and no friction) the spectrum of the streamfunction response agrees with that of the Rossby wave source up to a normalization constant. However, the two spectra diverge as $|V|$ increases due to its impact on ω_0. The most obvious effects are a reduction in the response at positive l and the emergence of a strong peak at the propagating wavenumber l_0. The eddy momentum flux cospectra in Fig. 4g show that the former is key to the reduction in the southward rotational momentum flux (thick blue line) when $|V|$ increases ($V = -1.5\,\mathrm{m\,s^{-1}}$ here) relative to the control resting state (thin blue line). The divergent momentum flux (red lines) is much less affected. The strong positive peak at the propagating wavenumber reflects the large contribution (sensitive to domain size) of this scale to the meridionally integrated momentum flux.

The above analysis implies that advection by the Hadley cell modulates the tilt of the rotational response, favoring modes that tilt westward in the direction of V ($Vl > 0$). When the large-scale divergence field is dominated by modes with $Vl < 0$, the tilt of the response and hence the rotational momentum fluxes weaken, or even reverse, with increasing $|V|$. The impact on the geopotential field with $V = -1.5\,\mathrm{m\,s^{-1}}$ can be appreciated in Fig. 4e. It is apparent that the geopotential tilt is much reduced compared to the $V = 0$ solution in Fig. 2a. Note that although the equatorial geopotential anomalies no longer vanish with nonzero V (zonal geopotential gradients can now be balanced by meridional momentum advection), the equatorial Kelvin wave is still very weak.

4. Newtonian cooling results

The sensitivity of the rotational eddy momentum fluxes to meridional flow uncovered in the previous section may help reconciling the conflicting results of Z19b and KH07 on the Hadley cell impact on tropical eddy momentum fluxes. Another factor that could play a role is the modulation of the eddy divergence field by the Hadley cell. As noted in the introduction, the eddy divergence is qualitatetively different in the simulations of KH07 with and without a Hadley cell. In this section we investigate the relevance of the above arguments when the divergence field is internally determined. The key questions that we address are the following. How is the divergence field internally determined in the full model? Can the meridional flow impact the divergent momentum flux through the modulation of the divergence field? To answer these questions, we add thermal damping to the previous setup and let the divergence field be internally determined forcing with a nontilted Q'.

Interestingly, inclusion of Newtonian damping makes the divergence field tilt eastward from the equator in both hemispheres as observed when the heating Q' does not tilt. This is shown in Fig. 5a for the solution with no friction and no meridional flow. Figure 5b describes in more detail the phase relation between D' and Q' for this solution and shows that D' leads Q' at all latitudes, with their phase difference increasing from 0 at the equator to $\pi/2$ at high latitudes (see also SP11). We can understand the phase lag between D' and Q' by noting that for a Rossby wave, we expect positive geopotential anomalies to the west of the divergence maximum and negative geopotential

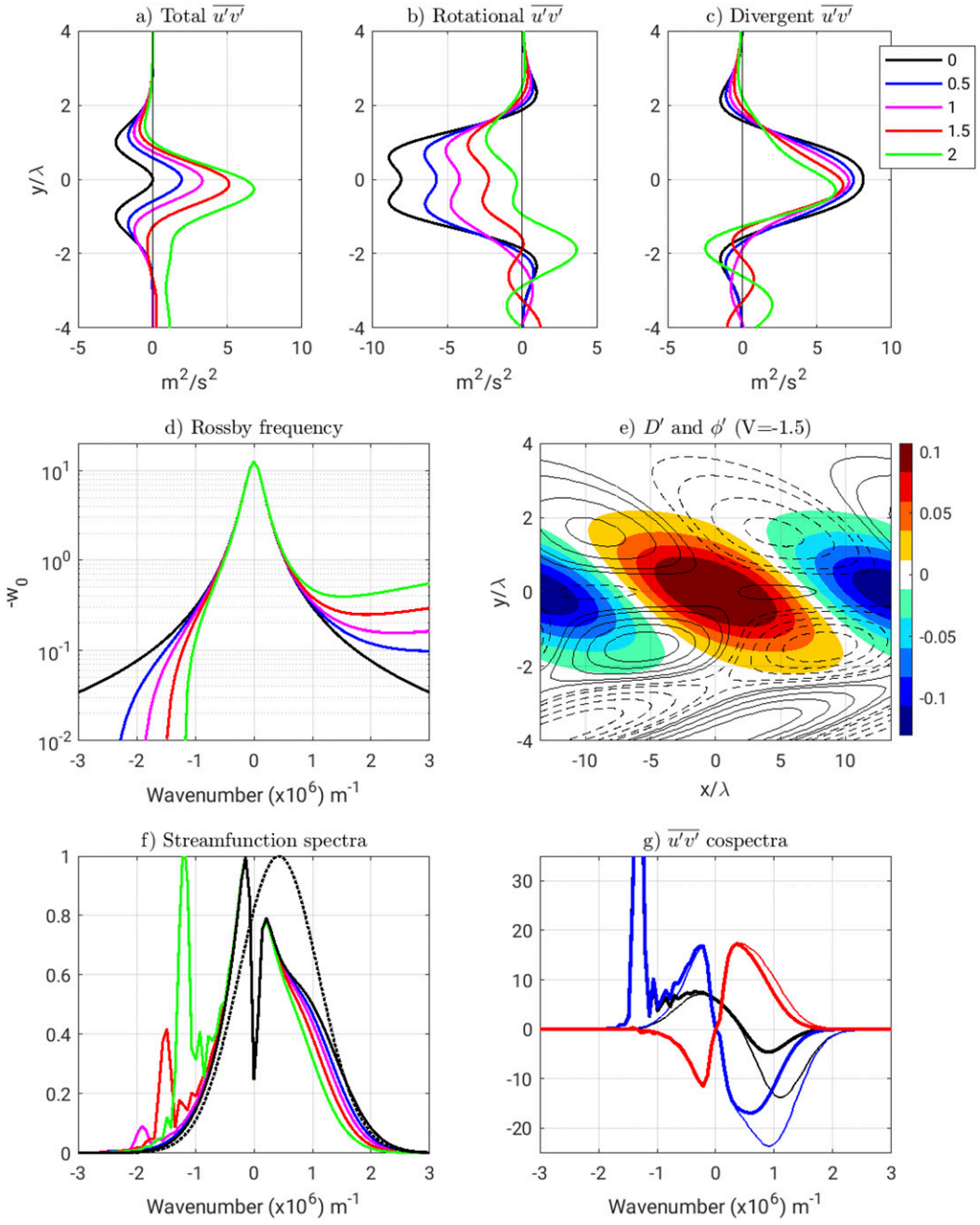

FIG. 4. (a) Total eddy momentum fluxes and (b) rotational and (c) divergent contributions in adiabatic, inviscid solutions with the control westward tilt and southward mean flow $V = 0$ (black), -0.5 (blue), -1 (magenta), -1.5 (red), and $-2\,\mathrm{m\,s^{-1}}$ (green). (d) Westward Rossby frequency ($\mathrm{day^{-1}}$) for $k = 1$ as a function of meridional wavenumber for the same values of V as in (a). (e) Divergence (shading) and geopotential (contours) for an adiabatic, inviscid problem with $V = -1.5\,\mathrm{m\,s^{-1}}$ and the control westward tilt. (f) Normalized meridional spectra for the divergence (black dotted), the divergent forcing (black solid), and the rotational streamfunction responses for the same solutions in (a). Note that with $V = 0$ the divergent-forcing and streamfunction spectra agree up to a normalization constant (black line). (g) Total eddy momentum flux cospectra (black lines) and rotational (blue lines) and divergent contributions (red lines) in adiabatic, inviscid solutions with the control westward tilt and no mean flow (thin) or $V = -1.5\,\mathrm{m\,s^{-1}}$ (thick).

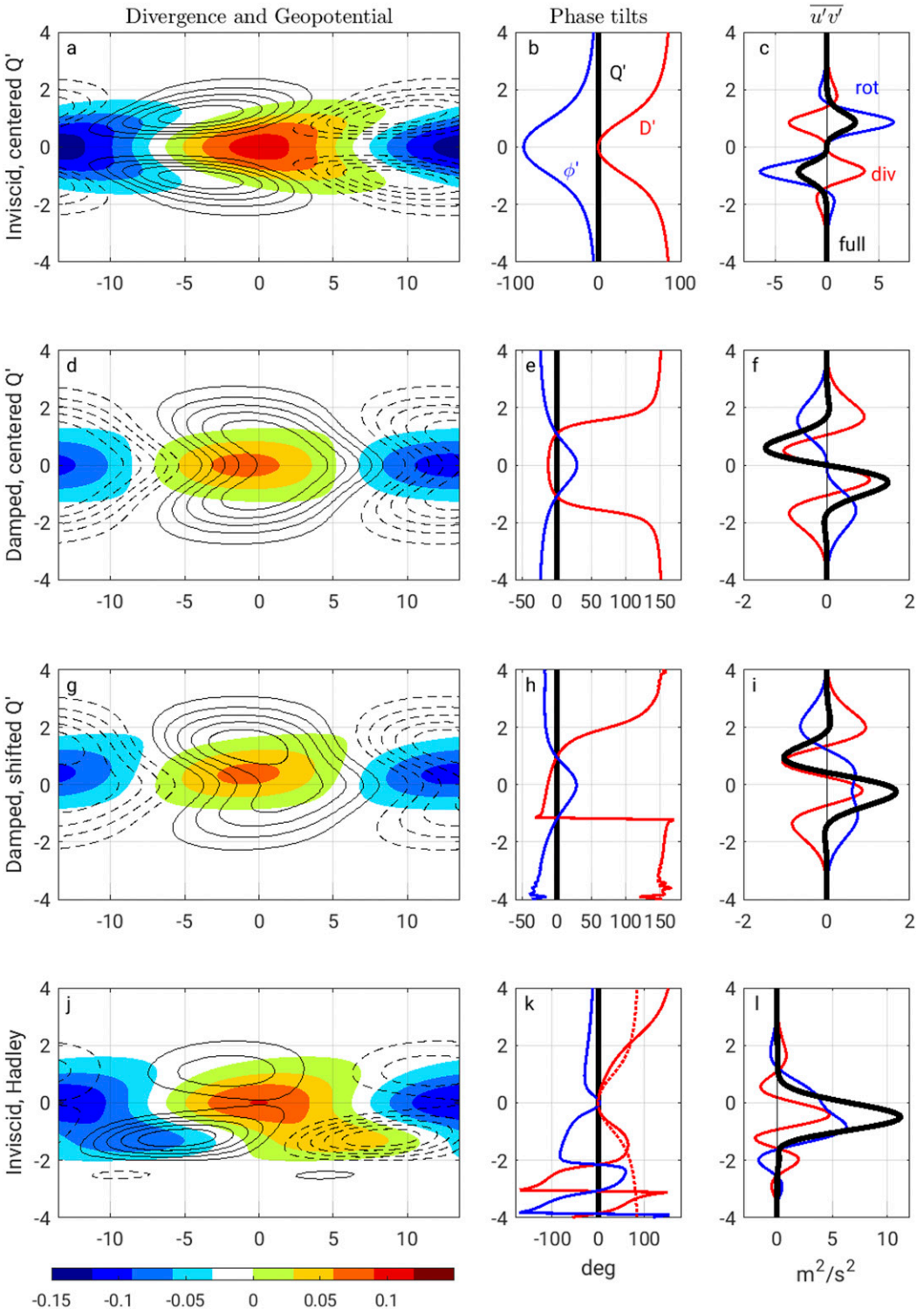

FIG. 5. (a) Divergence (shading; day^{-1}) and geopotential (contours; negative dashed) in an inviscid solution forced with nontilted heating and subject to the control thermal damping rate in a resting basic state. (b) For the same solution, phase shift of prescribed heating Q' (black), divergence D' (red), and geopotential ϕ' (blue) as a function of latitude. Positive (negative) values indicate phase leads (lags) relative to the phase of Q' at $y = 0$. (c) Total eddy momentum flux (black) and rotational (blue) and divergent (red) contributions for the same solution. (d)–(f) As in (a)–(c), but with the control friction. (g)–(i) As in (a)–(c), but with the control friction and shifted heating $y_0/\lambda = 0.5$. (j)–(l) As in (a)–(c), but with a southward mean flow $V = -1\,m\,s^{-1}$. The dotted red line in (k) shows the divergence phase tilt with no mean flow from (b) for comparison.

anomalies to the east. As a result, to the west of the D' maximum, Netwonian cooling compensates part of the prescribed heating Q' and $D' < Q'$, while to the east, Netwonian heating adds up to Q', leading to the observed eastward shift of D'. In this context, the eastward tilt of D' with latitude reflects the increasing impact of Newtonian cooling moving poleward (SP11, their appendix C).

Although the divergence field tilts in the right direction, the eddy momentum fluxes are very different from observations (Fig. 5c) for reasons discussed in section 3. As before, there is strong compensation between the rotational and divergent contributions to the eddy momentum flux, with the former dominating. This produces poleward eddy momentum fluxes in both hemispheres, indicating equatorward propagation of the off-equatorial Rossby waves. However, there can be no acceleration at the equator in this limit, as noted in section 3. When the symmetry of the problem is broken by tilting or shifting the heating the momentum flux becomes asymmetric but there is still no cross-equatorial propagation consistent with Sverdrup balance (not shown).

Friction has a profound impact on the solution by allowing a steady Kelvin wave response (Fig. 5d). Near the equator, the Kelvin response is associated with positive (negative) geopotential anomalies to the east (west) of the D' maximum. Using similar arguments to those above, it follows that D' must lag Q' over this region (Fig. 5e) in contrast with what we found for the Rossby response in the inviscid case. On the other hand, away from the equator we still observe a Rossby response with positive geopotential anomalies to the west of the divergence maximum, which implies that D' again leads Q' over this region. The westward (eastward) shift of D' relative to Q' near (away from) the equator is then associated with an eastward tilt of the divergence field moving poleward, most evident[2] in Fig. 5e. The phase lag between ϕ' and D' now exceeds $\pi/2$ at high latitudes, where the weak negative $\overline{\phi' D'}$ is associated with a conversion from kinetic to potential energy over regions with weak heating (see appendix B).

As discussed by SP11, the interaction between the Kelvin and Rossby waves produces equatorial eddy momentum flux convergence in this problem. Figure 5f shows that this convergence is due to $\overline{u_r' v_d'}$. When the symmetry is broken by shifting the heating off the equator (Fig. 5g), the response is associated with cross-equatorial eddy momentum flux into the forced hemisphere (Fig. 5i) as found in section 3a. However, the cross-equatorial eddy momentum flux is again very small.

Larger momentum fluxes are obtained when Sverdrup balance is violated through the addition of meridional flow. Figures 5j–l show the inviscid solution with $V = -1\ \mathrm{m\ s^{-1}}$. With no friction, the Kelvin response is very weak so that positive ϕ' anomalies are found westward of the D' maximum except very close to the equator. Consistent with this, the divergence field leads the heating Q', with the eastward D' shift increasing with latitude away from the equator in both hemispheres as in Fig. 5a. However, the divergence field is also affected by the meridional flow, becoming asymmetric about the equator. The divergence phase tilt is enhanced to the south of the equator and reduced to the north (cf. the solid and dotted red lines in Fig. 5k), and a secondary D' maximum appears at high southern latitudes collocated with regions of negative height (Fig. 5j). Since this divergence maximum extends beyond the forcing region, it must be forced by the circulation. As discussed in appendix B, the negative $\overline{\phi' D'}$ correlation is associated with a conversion from kinetic to potential energy. There are some similarities between this structure and the observed divergence (cf. Fig. 1) that cannot be captured by the WTG approximation.

Associated with these changes in the divergence field, there is now northward cross-equatorial divergent momentum flux. This stands in contrast with the results of Z19b, who found that $\overline{u_r' v_d'}$ was insensitive to V and vanished at the equator in his model *when the divergence field was kept fixed as V was changed* (see his Fig. 3f). On the other hand, the rotational eddy momentum flux $\overline{u_r' v_r'}$ is also directed northward and reinforces rather than cancels the divergent momentum flux at the equator (Fig. 5l), implying a violation of Sverdrup balance. This is possible because as another key difference from the $V = 0$ case, the geopotential phase lines now tilt in the opposite direction to the divergence instead of sharing the same tilt as in Fig. 5b.

Figure 6a describes the sensitivity of the two eddy momentum flux components when V is changed from -3 to $3\ \mathrm{m\ s^{-1}}$ with the control diabatic damping. Meridionally integrated, both $\langle \overline{u_r' v_r'} \rangle$ and $\langle \overline{u_r' v_d'} \rangle$ increase with (but point in the opposite direction to) V. For small $|V|$ the $\langle \overline{u_r' v_r'} \rangle$ changes dominate, but $\langle \overline{u_r' v_d'} \rangle$ becomes more important as $|V|$ increases. The cross-equatorial momentum fluxes

[2] With the large control value of friction, the Kelvin wave is so prominent that ϕ' is found to lie eastward of D' (so that D' lags Q') over a wide tropical region and the transition to westward ϕ' occurs over latitudes where the heating and divergence are already very weak. The subtle D' tilt in Fig. 5d becomes much more obvious with weaker friction and/or with broader Q' (not shown).

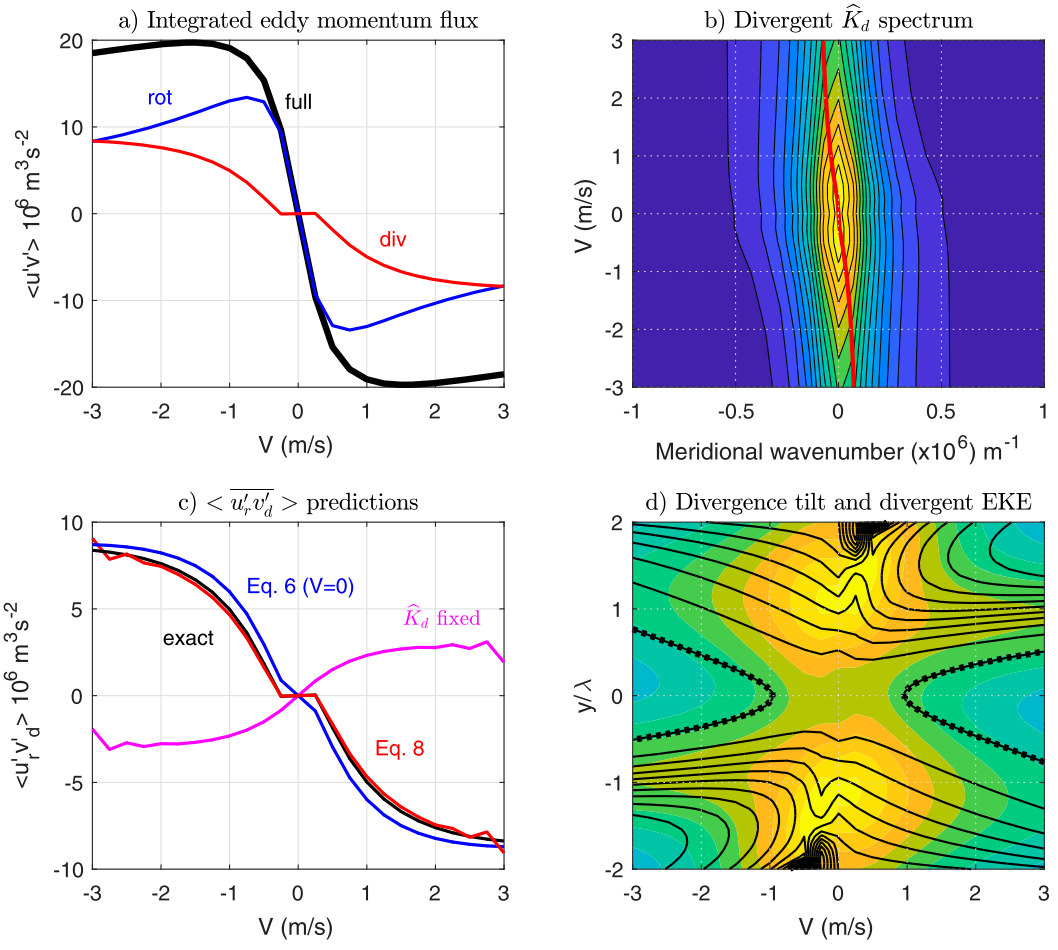

FIG. 6. (a) Sensitivity of the domain-integrated $\overline{u'_r v'_r}$ (blue), $\overline{u'_r v'_d}$ (red), and the full $\overline{u'v'}$ (black) to meridional flow. (b) Divergent eddy kinetic energy spectrum $\hat{K}_d(l)$ as a function of meridional flow. The thick red line shows the $\hat{K}_d$-weighted meridional wavenumber. (c) Divergent eddy momentum flux (black), estimate from Eq. (8) (red), and approximations using $V = 0$ and the simulated $\hat{K}_d$ (Eq. (6); blue) or the full weighting Eq. (8) with constant, symmetric $\hat{K}_d$ (magenta). (d) Divergent eddy kinetic energy (shading) and divergence phase shift (contoured every 10° with the zero contour dotted) as a function of latitude and meridional flow.

exhibit a similar dependence, but the divergent momentum flux catches up with $\langle \overline{u'_r v'_r} \rangle$ at smaller values of $|V|$ ($\approx 1\,\mathrm{m\,s^{-1}}$, not shown).

With nonzero V, Eq. (6) is no longer exact and must be replaced by (see appendix A):

$$\langle \overline{u'_r v'_d}(k) \rangle = \frac{2}{k} \int_{-\infty}^{\infty} l \alpha \hat{K}_d(k, l)\, dl, \tag{8}$$

where $\alpha = f(l/l_0)$ is a correcting factor that enhances the contribution of scales near l_0 to the integrated momentum flux. The sensitivity of $\langle \overline{u'_r v'_d} \rangle$ to V may arise from changes in this correcting factor with finite l_0 and/or from changes in the $\hat{K}_d$ spectrum. As shown in Fig. 6b, this spectrum shifts toward positive (negative) l with negative (positive) V, enhancing the eastward tilt of the divergence in the direction of V ($Vl < 0$).

Figure 6c shows that Eq. (8) (red line) reproduces very well the sensitivity of the simulated $\langle \overline{u'_r v'_d} \rangle$ (see appendix A for details of this calculation). We also show in this figure two different approximations. The blue line shows the predicted sensitivity using the simulated $\hat{K}_d$ spectrum and a constant $\alpha = 1$, equivalent to neglecting V and using Eq. (6). The prediction is quite good, suggesting that changes in the $\hat{K}_d$ spectrum with changing V play the dominant role for the simulated dependence. In contrast, the prediction computed using a V-dependent α with constant $\hat{K}_d$ (magenta line) displays the opposite $\langle \overline{u'_r v'_d} \rangle$ sensitivity.

In conclusion, our results support the argument of Z19b that the direction of the divergent momentum flux is determined by the meridional tilt of the divergence field, as measured by the K_d-weighted mean meridional wavenumber:

$$\tilde{l} = \frac{\int_{-\infty}^{\infty} l\hat{K}_d(k,l)\,dl}{\int_{-\infty}^{\infty} \hat{K}_d(k,l)\,dl}, \tag{9}$$

with the important caveat that this tilt is not independent of the circulation. The mean meridional wavenumber is shown as a function of V in Fig. 6b (thick red line). Inspection of the divergent response suggest two factors that may explain the $\tilde{l}$ sensitivity to V found in our simulations. First, inclusion of V makes the divergence tilt asymmetric about the equator as noted above, so that the divergence phase changes more rapidly in the downstream direction of V (Fig. 6d, contours). Additionally, K_d itself becomes equatorially asymmetric and also reaches its maximum in the downstream direction of V, over the region with rapid phase changes (Fig. 6d, shading).

5. Comparison with KH07

We next investigate the relevance of our findings for the eddy momentum flux sensitivity described by KH07 in nonlinear shallow-water simulations. The first question is whether our simple linear model can replicate their results. With this aim, we now use an inhomogeneous model with latitude-dependent $U(y)$, $V(y)$, and $H(y)$, diagnosed from the climatologies in Fig. 1 of KH07. We take into account the U structure to compute the background absolute vorticity and its gradient, and include the vorticity damping by the zonal-mean divergence $\partial_y V$. We use the same localized heating and the same frictional and diabatic time scales ($a^{-1} = b^{-1} =$ 10 days) as KH07. The only, important difference between the two models is our use of a linear beta-plane formulation.

Figure 7 shows results for some select KH07 cases: (i) a resting basic state with equatorially symmetric heating (cf. to their Figs. 2a,c), (ii) a solstitial basic state with equatorially symmetric heating (their Figs. 7a,c), (iii) a solstitial basic state with off-equatorial heating (their Figs. 7d,f), and (iv) a solstitial setting with no Hadley cell (their Fig. 9b). The left panels show the divergence and geopotential responses, using the same contour intervals and shading scheme as KH07 to facilitate the comparison. The center column of Fig. 7 shows the phase tilt for $k = 1$ (although KH07 use zonally localized heating, this zonal wave provides the dominant $\overline{u'v'}$ contribution), while the right column shows the eddy momentum flux by all waves.

Away from the equator, the agreement between the two models is remarkably good, both in structure and magnitude (except for the solstitial no-Hadley simulation). The main deficiency is found at the equator, where the Kelvin wave is nearly absent. This is consistent with the argument in section 3a relating the amplitude of the Kelvin wave response to friction, for KH07 use very weak friction. The stronger Kelvin wave in their simulations suggests that nonlinear advection is important for balancing the zonal pressure gradient at the equator in those simulations, consistent with the notion that nonlinearity provides the main source of friction in the tropics. This deficiency, however, does not seem to be important for the eddy momentum fluxes, which our model reproduces reasonably well. The failure of our model to capture the nearly symmetric KH07 response in the solstitial no-Hadley case suggests that friction/nonlinearity might be more important in the absence of a Hadley cell, consistent with the Sverdrup constraint.

KH07 did not separate the momentum fluxes into their rotational and divergent components. In our model, $\overline{u'_r v'_d}$ clearly dominates in agreement with observations. The weakness of the rotational component in these simulations compared to previous sections suggests that the inviscid, homogeneous model may exaggerate $\overline{u'_r v'_r}$. When a homogeneous, inviscid version of the solstitial KH07 simulation is implemented (setting U to zero and using a constant V and H characteristic of the solstitial state) the rotational momentum flux is much enhanced, while the divergent momentum flux has a similar magnitude (Figs. 8a–c). This simulation also exhibits a much more pronounced geopotential phase tilt than found in the inhomogeneous model.

Consistent with the dominance of the divergent component, the eddy momentum flux enhancement with a Hadley cell is almost entirely due to $\overline{u'_r v'_d}$, both with centered (Figs. 7a,d) and shifted (Figs. 7g,j) heating. Although the arguments in the previous section suggest that this enhancement might be associated with changes in the divergence tilt, the prominent southwest–northeast tilt seen south of the equator with a Hadley cell would seem more consistent with northward than with southward propagation. To clarify this issue, Fig. 8d isolates the $k = 1$ component of the solution, while Fig. 8e shows the coarse-grained divergence, filtered meridionally to retain only wavelengths longer than 4000 km ($|l| \leq 1.6 \times 10^{-6}\,\mathrm{m}^{-1}$). As in observations (see Fig. 1 and Z19b), the eastward divergence tilt moving away from the equator only becomes apparent with this filtering. Note that the bulk of the eddy momentum flux is due to these long scales, as shown by the meridional cospectra.

To investigate the impact of V in more detail, Fig. 8f shows the sensitivity of $\overline{u'v'}$ and its rotational and divergent components when the Hadley cell strength is varied. For these simulations we multiply the solstitial

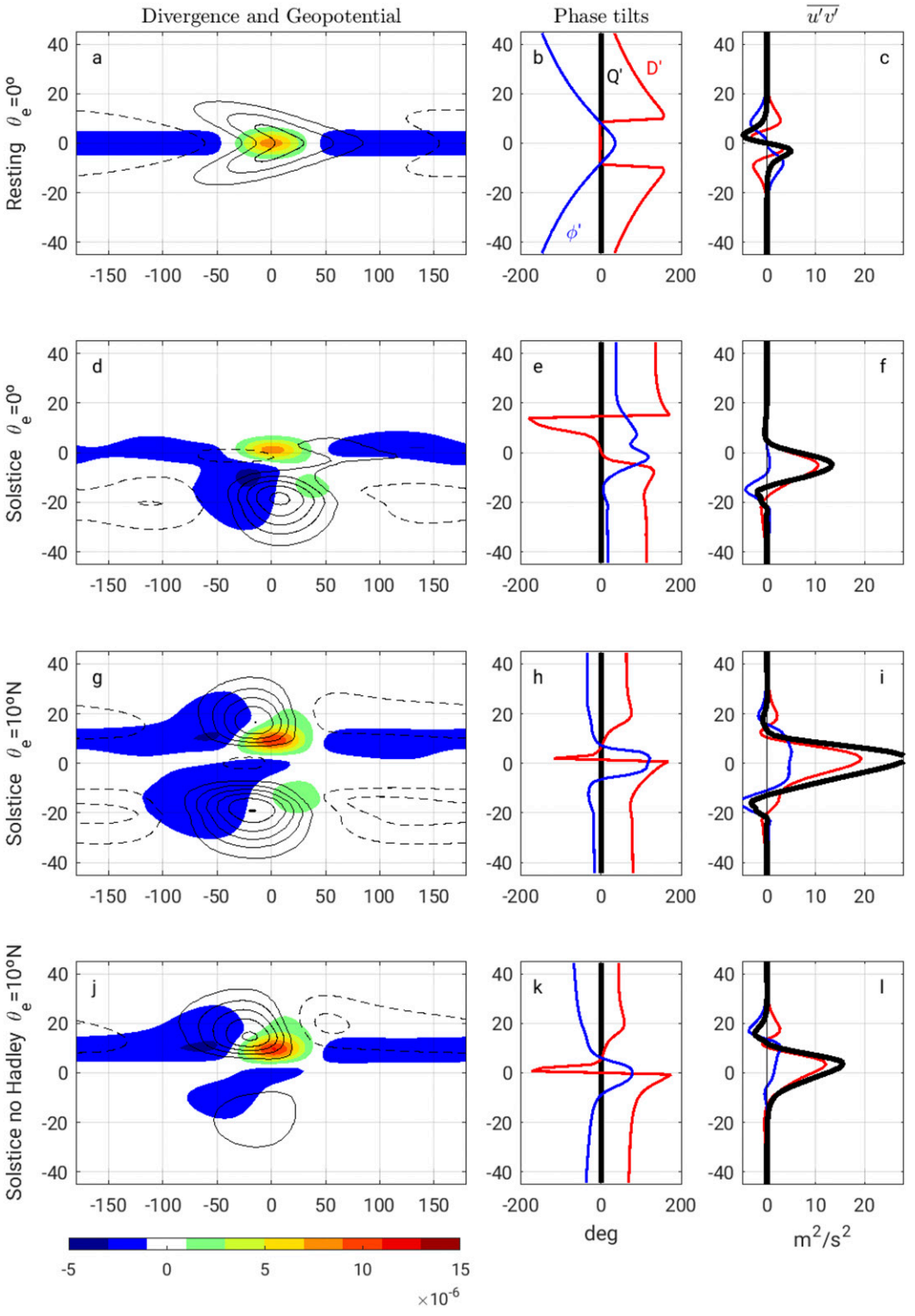

FIG. 7. As Figs. 5a–c, but for the following KH07 simulations: (a)–(c) resting basic state, equatorially symmetric heating (their Figs. 2a,c); (d)–(f) solstitial basic state, equatorially symmetric heating (their Figs. 7a,c); (g)–(i) solstitial basic state, heating shifted to 10°N (their Figs. 7d,f); and (j)–(l) solstitial zonal wind with no Hadley cell, heating shifted to 10°N (their Fig. 9b). The same contouring as in KH07 is used: divergence units are s^{-1}, with geopotential contours drawn every 5 min (a) and every 10 min all other panels. Note that the phase tilts are for $k = 1$ only. Momentum fluxes include contributions by all zonal waves.

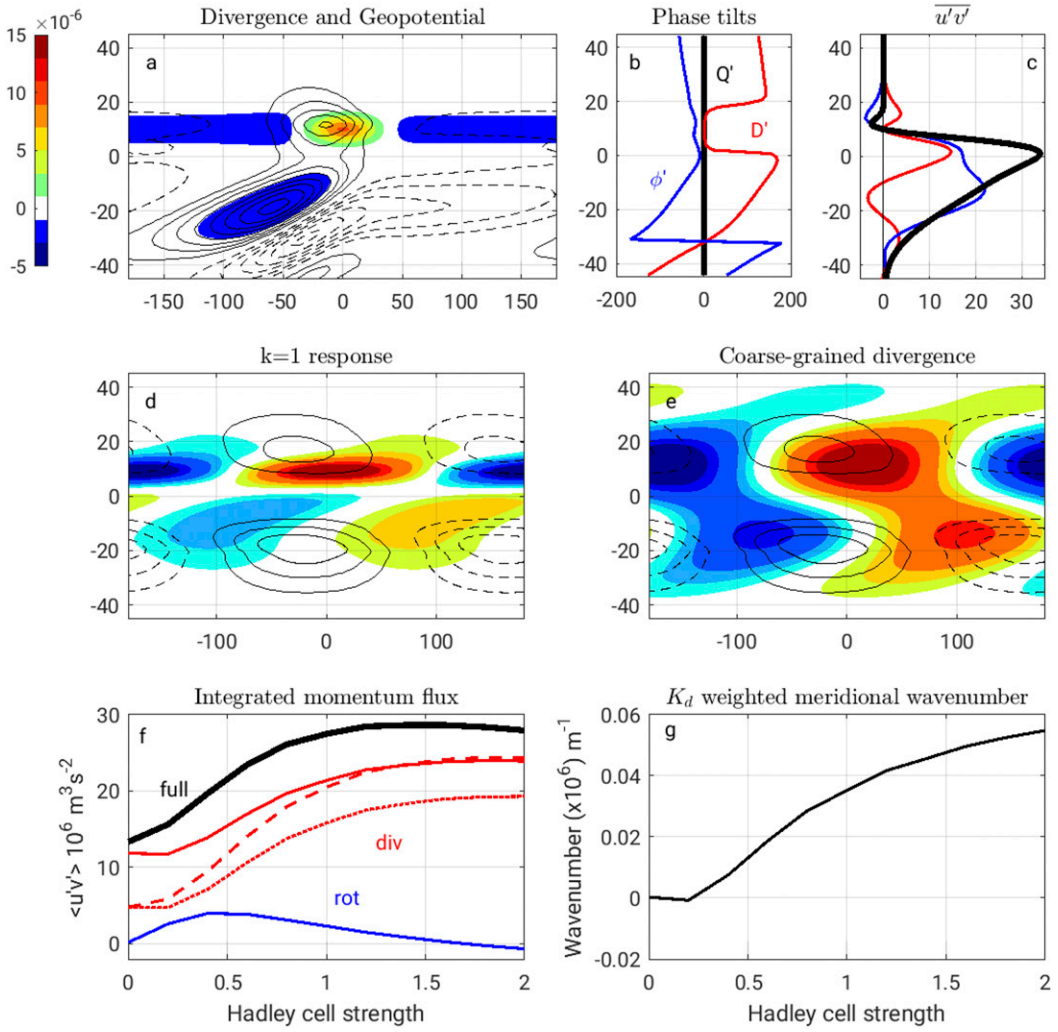

FIG. 8. (a)–(c) As Figs. 7g–i, but in an inviscid, homogeneous model with $U = 0$ and constant V. The geopotential contour is doubled (contours every 20 m). (d) As in Fig. 7g, but for the $k = 1$ zonal component. (e) As in (d), but filtered to retain only meridional wavelengths larger than 4000 km. (f) Sensitivity of the domain-integrated $\overline{u_r'v_r'}$ (blue), $\overline{u_r'v_d'}$ (red), and the full $\overline{u'v'}$ (black) in KH07's solstitial setting to Hadley cell strength, expressed as a fraction of the solstice climatology of V. The dashed red line shows the prediction using Eq. (8) with a homogeneous basic state; the dotted line is the same, but setting V to zero in Eq. (A11). (g) Sensitivity of the K_d-weighted meridional wavenumber to Hadley cell strength.

$V(y)$ of KH07 by a constant factor γ keeping everything else unchanged, with γ ranging from 0 to 2. The eddy momentum flux is more than doubled over this range, with the divergent component explaining the bulk of the change. We also show in this figure the prediction by Eq. (8) for a homogeneous model constructed taking the average V and vorticity gradient from 10°N to 30°S (dashed red line). This prediction can reproduce qualitatively the $\overline{u_r'v_d'}$ sensitivity, though it severely underestimates the momentum flux at low V. To assess the extent to which changes in the $\hat{K}_d$ spectrum are responsible for the $\overline{u_r'v_d'}$ sensitivity, we also show with dotted line in Fig. 8f a prediction neglecting the V contribution to α in Eq. (8) [friction is still included, essentially we take $r = 0$ in Eq. (A11)]. This prediction can capture the sensitivity of the momentum flux. The K_d-weighted meridional wavenumber $\tilde{l}$ [cf. Eq. (9)] is positive, consistent with the southeast–northwest tilt of the coarse-grained divergence, and increases with V in similar fashion (Fig. 8g).

6. Conclusions

This paper has investigated the dynamics of cross-equatorial eddy momentum transport in variants of the Gill model. We summarize our main findings below:

- We extended the analysis of Z19b on the relation between the sign of the divergent eddy momentum flux and the divergence phase tilt for a single wave to the case of a localized divergence field with a full meridional spectrum. We showed that in that case, the direction of the momentum flux depends on the sign of the mean meridional wavenumber weighted by the divergent eddy kinetic energy spectrum.
- In the absence of a vorticity source, Sverdrup balance represents a barrier to cross-equatorial propagation and the rotational and divergent momentum fluxes compensate. Two processes that may be important for violating Sverdrup balance and allowing cross-equatorial propagation are friction and meridional vorticity advection by the Hadley cell. Both processes are able to reduce or reverse the geopotential tilt imparted by a tilting divergent field, limiting the compensation by the rotational momentum fluxes.
- Away from the WTG limit, the heating is no longer locally balanced by the divergence. Newtonian cooling makes the divergence lag (lead) the heating for a Kelvin (Rossby wave). For the latter, the divergence phase lead increases with latitude as Newtonian cooling becomes more efficient balancing the heating poleward. This makes the divergence field tilt eastward with latitude as observed, though the relevance of this mechanism for the observed tilt is unclear because the heating is also affected by the circulation in a moist atmosphere.
- The divergence phase tilt is also affected by the mean meridional flow away from the WTG limit. With a Hadley cell, the eastward divergence tilt is enhanced in the downstream direction of the mean flow and the divergent eddy momentum flux increases in the opposite direction. Changes in the divergent momentum flux are well explained by the shift in the divergent eddy kinetic energy spectrum toward negative Vl.
- Our linear model reproduces reasonably well the nonlinear shallow-water results of Kraucunas and Hartmann (2007) when linearized about their climatology. The main deficiency of the linear model is the disappearance of the Kelvin wave with weak friction, as either friction or nonlinearity is needed to balance the zonal pressure gradient by the Kelvin wave. Despite this deficiency, the model can capture the eddy momentum fluxes of the nonlinear model. The sensitivity of the divergent momentum fluxes to the meridional flow in this model is consistent with the homogeneous theory, but the rotational momentum fluxes are much weaker.
- Our findings help reconcile the conflicting results of KH07 and Z19b on the sensitivity of cross-equatorial momentum transport to the Hadley cell. Consistent with KH07, the eddy momentum flux increases with Hadley cell strength in our model. This sensitivity was not observed by Z19b because the Hadley cell impacts the momentum transport through a modulation of the eddy divergence field, kept fixed in Z19b by virtue of the WTG approximation.

In conclusion, our analysis of the Gill model supports the arguments of Z19b that propagation from a tropical wave source is typically associated with an eastward tilt of the divergence in the direction of propagation. Z19b discussed this relation in the context of a single wave, and we have shown here that this relation also holds in an integral sense with localized heating. As a note of caution, this relation may not apply locally and may also not be obvious when the divergence field has fine meridional scale as shown in section 5. Additionally, the divergence field only tells part of the story when the rotational momentum fluxes are important.

As noted in the introduction, there is some evidence that the observed, robust eastward tilt of the divergence moving away from the equator is not forced by the geography. Indeed, idealized aquaplanet models appear to develop similar precipitation tilts when forced with untilted SST anomalies (see, e.g., Fig. 4 of Ting and Held 1990). Understanding what determines this tilt and its relation to propagation is an important open question. We have shown in this paper that Newtonian cooling alone can produce an eastward divergence tilt from the equator as observed, and that this tilt is enhanced in the downstream direction of a Hadley cell. However, it is likely that in the atmosphere the coupling between heating, moisture, and circulation plays the dominant role.

Acknowledgments. This work was motivated by comments and discussions with Ming Cai and Olivier Pauluis. I am grateful to Isaac Held for making me aware of the existence of the SPCZ as well as for sharing his insights on the tropical circulation. I am also grateful to the reviewers for comments that improved the content and clarity of this manuscript. A reviewer had a major impact on this work by stressing the role of the divergence changes for the momentum flux sensitivity, an aspect poorly emphasized in a first draft of the manuscript. She enlightened us on the sensitivity of the divergence tilt in the KH07 simulations and suggested the detailed comparison to their work in section 5. We acknowledge financial support by Grant CGL2015-72259-EXP by the State Research Agency of Spain and NSF funding for a summer visit to Princeton under Grant AGS-1733818.

APPENDIX A

Relation between the Divergent Eddy Kinetic Energy Spectrum and the $\overline{u_r'v_d'}$ Direction

Z19b discusses the relation between the $\overline{u_r'v_d'}$ direction and the meridional wavenumber l for a single wave. He shows that the sign of the momentum flux forced by the divergent advection of planetary vorticity, $\overline{u_r'v_d'}^{\beta}$, is opposite to that of $\omega_0 l$, where ω_0 is the free Rossby frequency. For waves with large meridional scales, the same is true for $\overline{u_r'v_d'}^{\mathrm{str}}$, the eddy momentum flux component forced by vortex stretching.

With localized heating, waves with different l contribute to the momentum transport. Depending on the sign of $\omega_0 l$, these contributions may or may not have the same sign as l. In this appendix, we derive an expression for the meridionally integrated momentum flux $\langle\overline{u_r'v_d'}\rangle$ as a weighted integral of the divergent eddy kinetic energy spectrum.

To derive this expression, consider the spectral form of the forced vorticity equation in a homogeneous basic state

$$-i\omega_0(k^2+l^2)\hat{\psi} = -\beta\hat{v}_d - \beta\widehat{yD}, \tag{A1}$$

where $\omega_0 = Uk + Vl - \beta k(k^2+l^2)^{-1}$. We may then express

$$\hat{u}_r = -il\hat{\psi} = -\frac{\beta l}{\omega_0(k^2+l^2)}(\hat{v}_d + \widehat{yD}). \tag{A2}$$

We can relate $\hat{v}_d$, $\hat{D}$, and $\widehat{yD}$ to the velocity potential $\hat{\chi}$:

$$\hat{v}_d = il\hat{\chi},$$
$$\hat{D} = -(k^2+l^2)\hat{\chi},$$
$$\widehat{yD} = i\frac{\partial\hat{D}}{\partial l} = -2il\hat{\chi} - i(k^2+l^2)\frac{\partial\hat{\chi}}{\partial l}.$$

The contributions of the different meridional modes to the integrated eddy momentum flux by zonal wave k can be written as

$$\langle\overline{u_r'v_d'}(k)\rangle = \int_{-L_y/2}^{L_y/2}\overline{u_r'v_d'}(k)\,dy = \int_{-\infty}^{\infty}C_k(l)\,dl, \tag{A4}$$

where $C_k(l) = \mathrm{Re}\{\hat{u}_r\hat{v}_d^*\}$ is the meridional cospectrum. We omitted for clarity constant factors involving the domain size and resolution associated with the Fourier-transform normalization.

Using the above definitions, we find

$$C_k(l) = \frac{\beta l}{\omega_0(k^2+l^2)}\mathrm{Re}\left\{l^2|\hat{\chi}|^2 + l(k^2+l^2)\frac{\partial\hat{\chi}}{\partial l}\hat{\chi}^*\right\} = \frac{\beta l^2}{\omega_0(k^2+l^2)}\frac{\partial\hat{K}_d}{\partial l}, \tag{A5}$$

where $\hat{K}_d = (1/2)(k^2+l^2)|\hat{\chi}|^2$ is the spectrum of divergent eddy kinetic energy.

Figure A1a shows that this prediction agrees very well with the simulated cospectrum for a sample simulation with $V = -3\,\mathrm{m\,s^{-1}}$ and the control diabatic damping. Figure A1b describes the cospectrum sensitivity to V predicted by this expression, also in excellent agreement with the numerical results (not shown). With nonzero V it is no longer true that the sign of the cospectrum is determined by l alone. As discussed by Z19b, with $Vl > 0$ and $|l|$ shorter than the resonant/propagating waveumber l_0, ω_0 changes sign and becomes eastward, and the divergent momentum flux has opposite sign to l. However, the contribution of this spectral region to $\langle\overline{u_r'v_d'}\rangle$ is very small—a large number of contours needs to be plotted in Fig. A1b to make this visible.

Note that although Eq. (A5) has a singularity at the resonant frequency $\omega_0 = 0$, the prediction is well behaved because $\partial\hat{K}_d/\partial l \to 0$ in a neighborhood of this point in the homogeneous model in the inviscid limit (not shown). Since these simulations do not incorporate any frictional damping (except for the sponge), the natural frequency is strictly real in this case.

Finally, we can integrate over all meridional wavenumbers to obtain

$$\langle\overline{u_r'v_d'}(k)\rangle = \int_{-\infty}^{\infty}\frac{\beta l^2}{\omega_0(k^2+l^2)}\frac{\partial\hat{K}_d}{\partial l}dl = \int_{-\infty}^{\infty}W(l)\hat{K}_d(k,l)\,dl, \tag{A6}$$

where $W(l) = -\partial/\partial l[\beta l^2/\omega_0(k^2+l^2)]$ is a weighting function.

With a resting basic state or when $\hat{K}_d(k,l)$ is concentrated at large scales so that we can approximate $\omega_0 \approx -\beta k(k^2+l^2)^{-1}$, the weighting function is particularly simple and we can write

$$\langle\overline{u_r'v_d'}(k)\rangle = \frac{2}{k}\int_{-\infty}^{\infty}l\hat{K}_d(k,l)\,dl, \tag{A7}$$

so that the sign of the divergent momentum flux is defined by the K_d-weighted meridional wavenumber. Figure 6c shows that this can provide a reasonable approximation even when $V \neq 0$.

More generally, if we neglect U and focus on long zonal waves, we expect $l \gg k$ for any l range for which V is not negligible. Thus, we can approximate

$$W(l) \approx -\frac{\partial}{\partial l}\left(\frac{\beta l^2}{Vl^3 - \beta k}\right) = \beta l\frac{Vl^3 + 2\beta k}{(Vl^3 - \beta k)^2} \tag{A8}$$

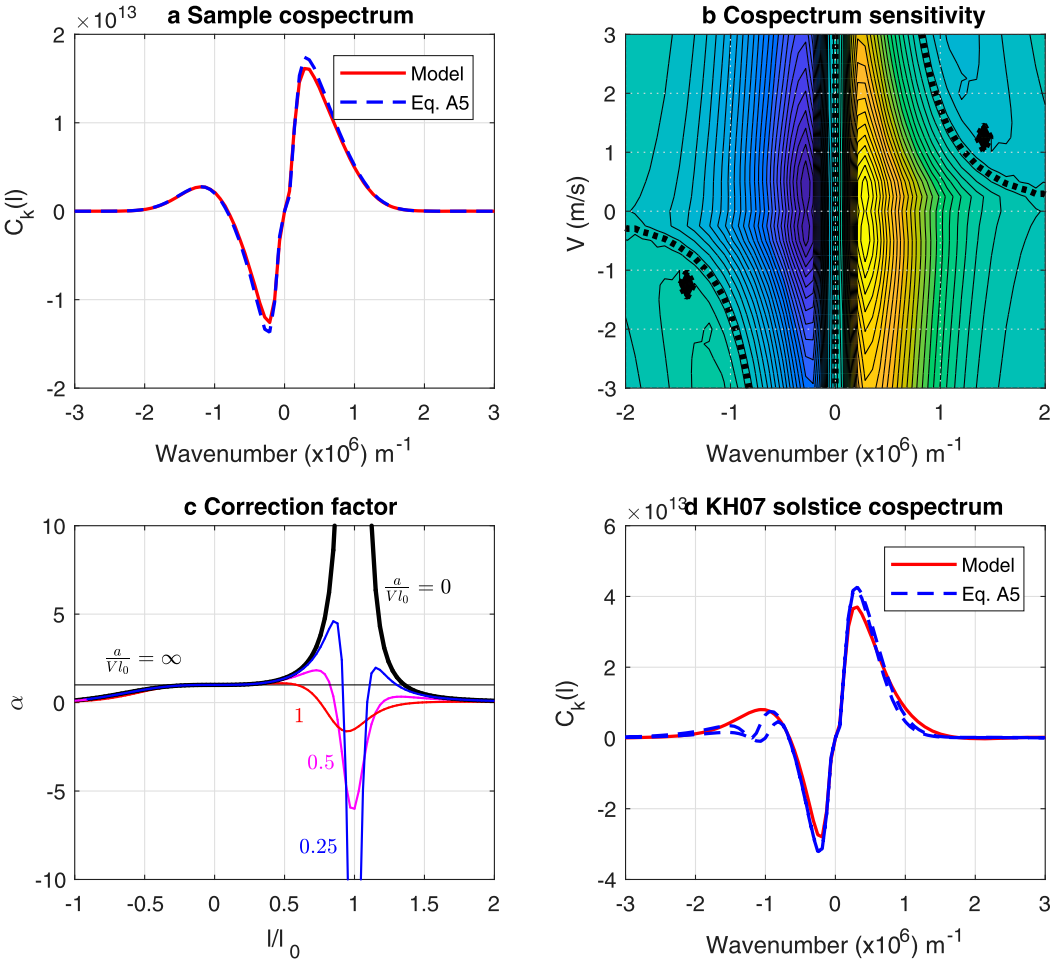

FIG. A1. (a) Model $\overline{u_r'v_d'}$ cospectrum for a simulation with the control diabatic damping and $V = -3\,\mathrm{m\,s^{-1}}$ (solid red) and prediction by Eq. (A5) (dashed blue). (b) Sensitivity of the cospectrum when V is varied predicted by Eq. (A5). (c) Correcting factor $\alpha(l/l_0)$ in Eq. (A11) for selected values of the nondimensional friction parameter $a/(Vl_0)$. The limit $a/(Vl_0) \to \infty$ (corresponding to $V = 0$) is given by the horizontal line $\alpha = 1$. (d) Model $\overline{u_r'v_d'}$ cospectrum for KH07's solstitial setting (red) and predictions by Eq. (A5) (dashed blue) using two different homogeneous basic states (see text for details).

so that Eq. (A7) is replaced by

$$\langle \overline{u_r'v_d'}(k) \rangle = \frac{2}{k}\int_{-\infty}^{\infty} l\alpha(l/l_0)\hat{K}_d(k,l)\,dl, \qquad \text{(A9)}$$

where $\alpha(l/l_0)$ is a correcting factor defined by

$$\alpha = \frac{1}{2}\frac{r+2}{(r-1)^2}, \qquad \text{(A10)}$$

where $r = Vl^3/(\beta k) = (l/l_0)^3$, with $l_0 = (\beta k/V)^{1/3}$ the resonant wavenumber. This expression is shown with thick black line in Fig. A1c. Since the correcting factor is generally positive, it is still true that the sign of the momentum flux is determined by the weighted meridional tilt. But with nonzero V, the contribution by modes with large $|l|$ is reduced, while contributions near the resonant frequency are greatly enhanced.

In fact, the integral using this weighting no longer converges due to the increased order of the singularity and the fact that unlike $\partial\hat{K}_d/\partial l$, the divergent eddy kinetic energy does not strictly vanish at the resonant frequency. One way to deal with this singularity is to add some frictional damping a and make this damping suitably small. More generally, we would also like to generalize our results for the dissipative case.

With nonzero a, the Rossby frequency ω_0 is imaginary. In that case, the cospectrum $C_k(l) = \mathrm{Re}\{\hat{u}_r\hat{v}_d^*\}$ cannot be expressed in terms of $\hat{K}_d$ alone and also depends on the slope (in l space) of the $\hat{\chi}(l)$ phase lines. However, when a is small this dependence can be neglected and the

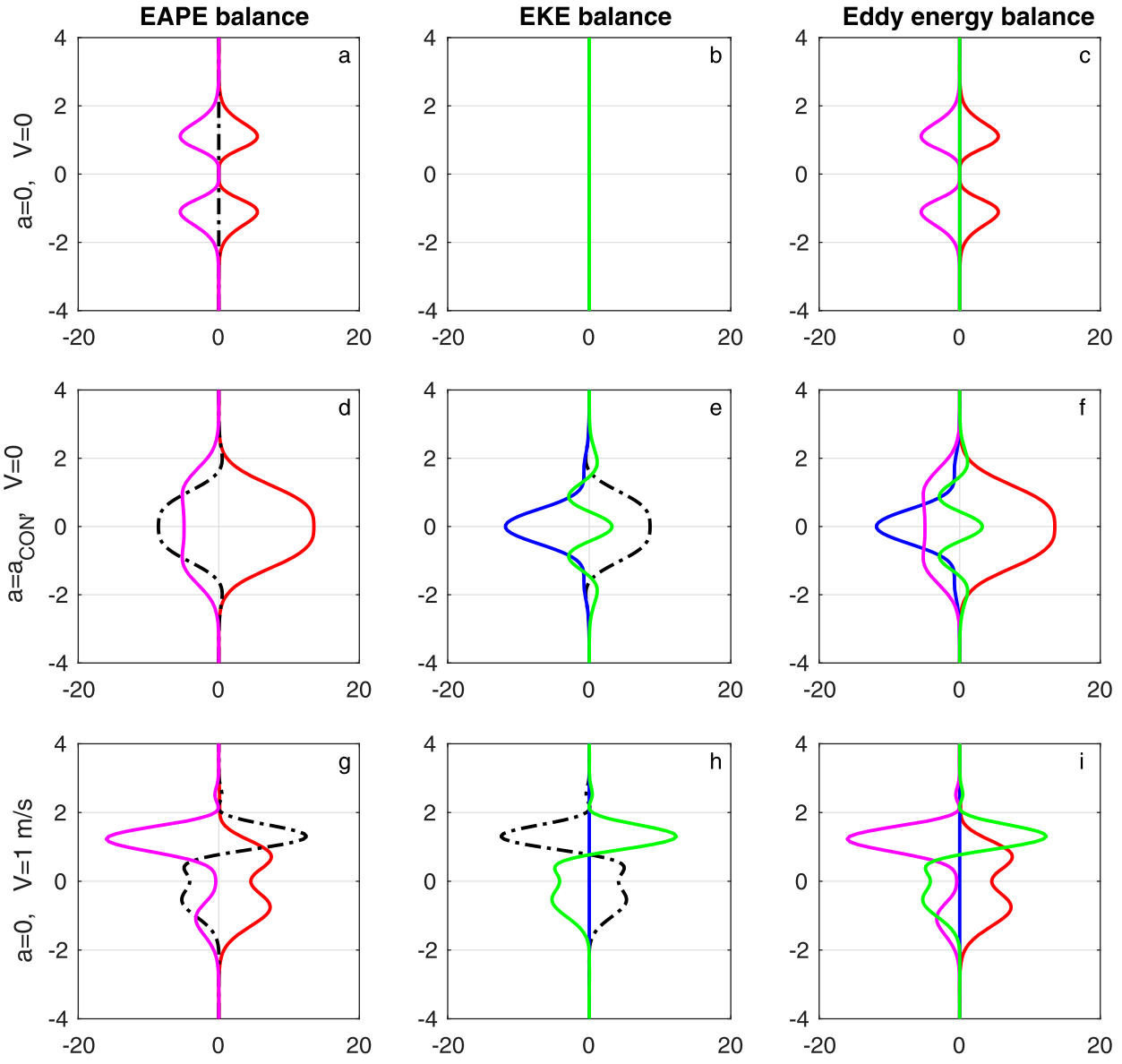

FIG. B1. (a) EAPE balance as a function of latitude for the inviscid solution with no mean flow. The red line is the diabatic forcing, the dash–dotted black line the EAPE–EKE conversion and the magenta line the diabatic dissipation. (b) EKE balance for the same problem. The blue line is the frictional dissipation and the green line is the combined EKE redistribution by the Hadley cell and pressure force (wave flux term). (c) Total eddy energy balance. (d)–(f) As in (a)–(c), but with the control friction. (g)–(i) As in (a)–(c), but with a mean flow $V = 1\,\mathrm{m\,s^{-1}}$. Units are $\mathrm{J\,kg^{-1}\,day^{-1}}$ in all panels.

above derivation is easily generalized to produce the following α:

$$\alpha = \frac{(r+2)[(r-1)^2 - f^2]}{2[(r-1)^2 + f^2]^2}, \tag{A11}$$

where $f = al^2/(\beta k) = a/(Vl_0)r^{2/3}$. Figure A1c shows the structure of α for a few choices of the dimensionless damping parameter $a/(Vl_0)$. The red line in Fig. 6c, computed using a frictional time scale $a^{-1} = 20$ days, produces nearly perfect agreement with the inviscid model $\langle \overline{u_r' v_d'} \rangle$.

The main limitation of the diagnostics presented above is the assumption of a homogeneous basic state with constant U, V, and β. However, the diagnostics still work reasonably well in the more realistic, nonhomogeneous situations studied by KH07. This is illustrated in Fig. A1d for KH07's solstitial setting with shifted heating. The red line shows the model cospectrum $C_k(l)$ and the two blue dashed lines show predictions based on

Eq. (A5) using two different homogeneous basic states (the maximum southward V and an equatorial β, or the mean V and absolute vorticity gradient averaged within 10° of the equator). The two predictions are similar and reproduce reasonably well the model results [the largest differences, near the resonant frequency, are in fact due to neglecting the imaginary component of ω_0 in the derivation of Eq. (A5)]. Despite some errors, Fig. 8f shows that Eq. (A9) can capture qualitatively the sensitivity of the divergent momentum flux to the mean flow in the inhomogeneous model.

APPENDIX B

Energy Conversions and the ϕ'–D' Phase Lag

In this appendix, we discuss the closure of the eddy energy balance and its relationship with the ϕ'–D' phase lag. As discussed in section 4, this lag has implications for the determination of the divergence phase tilt.

We first derive an equation for eddy kinetic energy (EKE) density by combining the two momentum equations [Eqs. (1a) and (1b)] in the usual way. This gives

$$-V\frac{\partial \mathrm{EKE}}{\partial y}-\frac{\partial \overline{v'\phi'}}{\partial y}+\overline{D'\phi'}-2a\mathrm{EKE}=0, \qquad \text{(B1)}$$

where $\mathrm{EKE}=(\overline{u'^2}+\overline{v'^2})/2$ is eddy kinetic energy density. Similarly, we can derive an equation for eddy available potential energy (EAPE) density using the continuity equation [see Eq. (1c)]:

$$\overline{Q'\phi'}-\overline{D'\phi'}-2b\mathrm{EAPE}=0, \qquad \text{(B2)}$$

where $\mathrm{EAPE}=\overline{\phi'^2}/(2c^2)$. The potential energy generated by the heating Q' can be dissipated diabatically or converted into eddy kinetic energy and then dissipated by friction (possibly nonlocally). The well-known role of $\overline{D'\phi'}$ as an EAPE to EKE conversion term implies that we can understand the sign of this term (and hence the $\phi'-D'$ phase relation) using the energy cycle.

For instance, consider the inviscid limit $a=0$. In this limit, all the eddy dissipation must be diabatic. When $V=0$ too, the zonal momentum equation [Eq. (1a)] implies that $\overline{v'\phi'}=0$ and hence neither the mean flow nor the wave flux can redistribute EKE. In this limit, $\overline{D'\phi'}=0$ and D' and ϕ' are in quadrature (Fig. 5b). All the EAPE generated by the heating is dissipated locally by Newtonian cooling (Fig. B1a) and the phase shift between Q' and D' increases with Newtonian dissipation as discussed in section 4.

With nonzero a, we expect part of the EAPE generatedy by the heating to be converted into EKE and dissipated by friction, hence a positive $\overline{D'\phi'}>0$. This requires the phase lag between D' and ϕ' to be less than $\pi/2$ whether D' leads ϕ' (as for a Rossby wave) or lags it (as for a Kelvin wave). This is the case over most of the domain in Figs. 5e and 5h. However, in both cases rapid changes in the phase of D' are found on the sides and the $D'-\phi'$ phase lead appears to asymptote π at large distance. Figures B1d–f show the EKE, EAPE and total eddy energy balance for the solution in Fig. 5d. Although $\overline{D'\phi'}>0$ over most of the domain, there is (weak) EKE to EAPE conversion ($\overline{D'\phi'}<0$) on the sides, where diabatic dissipation is more important than frictional dissipation. This is possible because of the EKE redistribution by the pressure gradient force (wave flux term), which provides an EKE source over this region. However, since the wave flux EKE redistribution is weak the change in sign of $\overline{D'\phi'}$ occurs over latitudes with very weak amplitude.

Finally, we can also get nonzero $\overline{D'\phi'}$ with $a=0$ in the presence of a Hadley cell. In that case, $\overline{D'\phi'}$ only vanishes in a domain average and there is EKE transport (by both the Hadley cell and $\overline{v'\phi'}$) from regions of EAPE to EKE conversion to regions of EKE to EAPE conversion (Fig. B1h). Because $\overline{D'\phi'}$ vanishes in a domain average, the negative $\overline{D'\phi'}$ (corresponding to a D'–ϕ' phase lag between $\pi/2$ and π) is now observed over regions with significant eddy amplitude. This is manifested in Fig. 5j in the form of a second divergence maximum at high negative latitudes collocated with regions of negative height.

REFERENCES

Bretherton, C. S., and A. H. Sobel, 2003: The Gill model and the weak temperature gradient approximation. *J. Atmos. Sci.*, **60**, 451–460, https://doi.org/10.1175/1520-0469(2003)060<0451:TGMATW>2.0.CO;2.

Dee, D. P., and Coauthors, 2011: The ERA-Interim reanalysis: Configuration and performance of the data assimilation system. *Quart. J. Roy. Meteor. Soc.*, **137**, 553–597, https://doi.org/10.1002/qj.828.

Dima, I. M., J. M. Wallace, and I. Kraucunas, 2005: Tropical zonal momentum balance in the NCEP reanalyses. *J. Atmos. Sci.*, **62**, 2499–2513, https://doi.org/10.1175/JAS3486.1.

Gill, A., 1980: Some simple solutions for heat-induced tropical circulation. *Quart. J. Roy. Meteor. Soc.*, **106**, 447–462, https://doi.org/10.1002/qj.49710644905.

Held, I. M., 1999: Equatorial superrotation in Earth-like atmospheric models. *Bernhard Haurwitz Memorial Lecture*, Amer. Meteor. Soc., 24 pp., https://www.gfdl.noaa.gov/wp-content/uploads/files/user_files/ih/lectures/super.pdf.

Kraucunas, I., and D. L. Hartmann, 2005: Equatorial superrotation and the factors controlling the zonal-mean zonal winds in the tropical upper troposphere. *J. Atmos. Sci.*, **62**, 371–389, https://doi.org/10.1175/JAS-3365.1.

——, and ——, 2007: Tropical stationary waves in a nonlinear shallow-water model with realistic basic states. *J. Atmos. Sci.*, **64**, 2540–2557, https://doi.org/10.1175/JAS3920.1.

Laraia, A. L., and T. Schneider, 2015: Superrotation in terrestrial atmospheres. *J. Atmos. Sci.*, **72**, 4281–4296, https://doi.org/10.1175/JAS-D-15-0030.1.

Lee, S., 1999: Why are the climatological zonal winds easterly in the equatorial upper troposphere? *J. Atmos. Sci.*, **56**, 1353–1363, https://doi.org/10.1175/1520-0469(1999)056<1353:WATCZW>2.0.CO;2.

Li, Y., J. Li, F. F. Jin, and S. Zhao, 2015: Interhemispheric propagation of stationary Rossby waves in a horizontally nonuniform background flow. *J. Atmos. Sci.*, **72**, 3233–3256, https://doi.org/10.1175/JAS-D-14-0239.1.

Matsuno, T., 1966: Quasi-geostrophic motions in the equatorial area. *J. Meteorol. Soc. Japan*, **44**, 25–43, https://doi.org/10.2151/JMSJ1965.44.1_25.

Merlis, T. M., and T. Schneider, 2010: Atmospheric dynamics of Earth-like tidally locked aquaplanets. *J. Adv. Model. Earth Syst.*, **2** (4), https://doi.org/10.3894/JAMES.2010.2.13.

Neelin, J. D., 1988: A simple model for surface stress and low-level flow in the tropical atmosphere driven by prescribed heating. *Quart. J. Roy. Meteor. Soc.*, **114**, 747–770, https://doi.org/10.1002/qj.49711448110.

Schneider, E. K., and I. G. Watterson, 1984: Stationary Rossby wave propagation through easterly layers. *J. Atmos. Sci.*, **41**, 2069–2083, https://doi.org/10.1175/1520-0469(1984)041<2069:SRWPTE>2.0.CO;2.

Shaw, T. A., 2014: On the role of planetary-scale waves in the abrupt seasonal transition of the Northern Hemisphere general circulation. *J. Atmos. Sci.*, **71**, 1724–1746, https://doi.org/10.1175/JAS-D-13-0137.1.

Showman, A. P., and L. M. Polvani, 2010: The Matsuno-Gill model and equatorial superrotation. *Geophys. Res. Lett.*, **37**, L18811, https://doi.org/10.1029/2010GL044343.

——, and ——, 2011: Equatorial superrotation on tidally locked exoplanets. *Astrophys. J.*, **738**, 71, https://doi.org/10.1088/0004-637X/738/1/71.

Sobel, A. H., J. Nilsson, and L. M. Polvani, 2001: The weak temperature gradient approximation and balanced tropical moisture waves. *J. Atmos. Sci.*, **58**, 3650–3665, https://doi.org/10.1175/1520-0469(2001)058<3650:TWTGAA>2.0.CO;2.

Suarez, M. J., and D. G. Duffy, 1992: Terrestrial superrotation: A bifurcation of the general circulation. *J. Atmos. Sci.*, **49**, 1541–1554, https://doi.org/10.1175/1520-0469(1992)049<1541:TSABOT>2.0.CO;2.

Ting, M., and I. M. Held, 1990: The stationary wave response to a tropical SST anomaly in an idealized GCM. *J. Atmos. Sci.*, **47**, 2546–2566, https://doi.org/10.1175/1520-0469(1990)047<2546:TSWRTA>2.0.CO;2.

Vallis, G. K., 2017: *Atmospheric and Oceanic Fluid Dynamics*. Cambridge University Press, 946 pp.

Van Der Wiel, K., A. J. Matthews, D. P. Stevens, and M. M. Joshi, 2015: A dynamical framework for the origin of the diagonal South Pacific and South Atlantic convergence zones. *Quart. J. Roy. Meteor. Soc.*, **141**, 1997–2010, https://doi.org/10.1002/qj.2508.

——, ——, M. M. Joshi, and D. P. Stevens, 2016: Why the South Pacific convergence zone is diagonal. *Climate Dyn.*, **46**, 1683–1698, https://doi.org/10.1007/s00382-015-2668-0.

Zurita-Gotor, P., 2019a: The role of the divergent circulation for large-scale eddy momentum transport in the tropics. Part I: Observations. *J. Atmos. Sci.*, **76**, 1125–1144, https://doi.org/10.1175/JAS-D-18-0297.1.

——, 2019b: The role of the divergent circulation for large-scale eddy momentum transport in the tropics. Part II: Dynamical determinants of the momentum flux. *J. Atmos. Sci.*, **76**, 1145–1161, https://doi.org/10.1175/JAS-D-18-0304.1.

——, and I. M. Held, 2018: The finite-amplitude evolution of mixed Kelvin–Rossby wave instability and equatorial superrotation in a shallow-water model and an idealized GCM. *J. Atmos. Sci.*, **75**, 2299–2316, https://doi.org/10.1175/JAS-D-17-0386.1.